Reducing effects of particle adsorption to the air-water interface in cryoEM

Alex J. Noble[1,†], Hui Wei[1,†], Venkata P. Dandey[1,†], Zhening Zhang[1], Clinton S. Potter[1,2], Bridget Carragher[1,2,*]

[†]These authors contributed equally to this work
*Corresponding author

Affiliations:

[1]National Resource for Automated Molecular Microscopy, Simons Electron Microscopy Center, New York Structural Biology Center, New York, United States

[2]Department of Biochemistry and Molecular Biophysics, Columbia University, New York, United States

Abstract

Most protein particles prepared in vitreous ice for single particle cryo-electron microscopy are adsorbed to air-water or substrate-water interfaces, potentially causing particles to adopt preferred orientations. Using the Spotiton robot and nanowire grids, we can significantly reduce air-water interface issues by decreasing the dwell time of particles in thin liquid films. We demonstrate this by using single particle cryoEM and cryoET on three biological samples.

Single particle cryo-electron microscopy (cryoEM) allows for the structural study of purified proteins in solution to near-atomic resolutions[1,2]. Proteins are preserved in their hydrated state by spreading the sample out in a thin layer of buffer solution supported on a cryoEM grid and rapidly plunging the grid into a cryogen so as to convert the liquid layer into vitreous ice[3,4]. Alignment, classification, and reconstruction of a sufficient number of EM images of randomly oriented protein particles provides 3D density maps. Advances in electron microscope hardware, cameras, and image processing methods have enabled cryoEM as a method for reconstructing a wide range of protein complexes to near-atomic resolution in near-native conditions in multiple functional states[5,6].

Tomographic studies of a wide range of single particle samples have shown that the vast majority of proteins prepared over holey substrates using standard vitrification methods are adsorbed to air-water interfaces[7]. This has the potential to cause the protein particles to adopt preferred orientations as well as the possibility of damaging or degrading the protein structure[7,8]. There are various options for avoiding contact with the air-water interface and its potential deleterious effects, including using surfactants as a barrier, sequestering the particles to a support film[8], or by outrunning some of the surface effects by reducing the length of time that the sample dwells in the thin liquid film prior to vitrification. It is this latter approach that we describe here; if the dwell time is reduced sufficiently, the particles in solution may either not have time to diffuse completely to the air-water or substrate-water interfaces or may not have fully equilibrated after having diffused there to the air-water interface, depending on their affinity for the interfaces.

For most cryoEM vitrification devices (FEI Vitrobot, Gatan CP3, Leica EM GP, manual plungers) the time that elapses between the wicking of a sample to a thin film and the grid entering the cryogen is typically on the order of 1 second or greater. Assuming a thin film of thickness ~100nm, various estimates indicate that the protein particles will collide with an air-water interface about 100-1000 times during this time interval[9,10], providing ample opportunity for adsorption and preferential orientation. There are at least two devices currently under development that allow for much more rapid plunge-freezing: a microfluidic spray-plunging machine developed by the Frank group[11], and Spotiton, a robotic device that dispenses picoliter-volumes of sample onto a self-blotting nanowire grid as it flies past *en route* to vitrification[12–15]. The time interval between sample application to the grid and vitrification is called the spot-to-plunge time. Previously, the spot-to-plunge times on the Spotiton robot were on the order of 500 ms or more, but we recently modified the device to achieve spot-to-plunge times on the order of 100 ms.

Here we demonstrate, using three different specimens (hemagglutinin, insulin receptor bound to insulin[16], and apoferritin), that by decreasing the spot-to-plunge time and thus reducing the dwell time of the sample in the thin liquid layer, the interaction of the particles with the air-water interfaces may be altered. We used Spotiton to vitrify samples with spot-to-plunge times of 100-200 ms and compared these results, using cryoEM and cryoET[7], to those with spot-to-plunge times of 400-800 ms, serving as controls.

With longer spot-to-plunge times (600-800 ms), hemagglutinin exhibits severe preferred orientation, presenting only a single top view of the particle in 2D class averages (**Fig. 1a**), while 2D class averages of insulin-bound insulin receptor provide a limited set of particle orientations (**Fig. 1a**). For both samples, the vast majority of particles are closely associated with the air-

water interfaces (**Supplementary Videos 1 & 2**). As a consequence of the preferred orientation, coherent initial models of hemagglutinin and insulin receptor could not be generated and isotropic 3D reconstructions could not be obtained unless micrographs were acquired with the grid tilted relative to the electron beam[17], which however imposes collection, processing, and resolution limitations. Apoferritin with 0.5 mM TCEP (15 mg/mL = 20,530 particles/μm^3 in solution), when plunged with a longer spot-to-plunge time of 500 ms, primarily adsorbs to the air-water interfaces, although its high symmetry and the prevalence of local tilt in exposure areas[7] effectively negate any issues of preferred orientation (**Fig. 2a**, **Supplementary Video 3**). The volume of ice occupied by the non-adsorbed apoferritin particles contains a particle density of about 1,668 particles/μm^3 (**Supplementary Fig. 1**).

A shorter spot-to-plunge time of 100 ms for hemagglutinin results in dramatically reduced preferred orientations (**Fig. 1b**), providing a 3D reconstructed map at 3.8 Å (**Fig. 1c**) that is more isotropic and better resolved compared to the 4.2 Å map[17] produced using grid tilt. Similarly, for the insulin-bound insulin receptor with a spot-to-plunge time of 200 ms, the reduced preferred orientation provides additional critical views of the complex (**Fig. 1b**), producing a 4.9 Å 3D reconstruction (**Fig. 1d**) that is of higher quality and more isotropic than that derived from images of tilted specimen[16] (**Supplementary Fig. 2**). While the preferred orientation of hemagglutinin and insulin receptor were each significantly reduced with shorter spot-to-plunge times, the majority of particles still remained adsorbed to the air-water interfaces (**Supplementary Videos 4 & 5**). However, in the case of apoferritin with TCEP, a spot-to-plunge time of 170 ms vs. 500 ms significantly increased the density of non-adsorbed particles (**Fig. 2b**, **Supplementary Video 6**). The density of particles not adsorbed to the air-water interfaces increased by a factor of ~20x to about 31,725 particles/μm^3 (**Supplementary Fig. 3**). When apoferritin at a lower concentration was prepared without TCEP (6 mg/mL = 8,212 particles/μm^3 in solution), the density of non-adsorbed particles increased from about 3,043 particles/μm^3 with a spot-to-plunge time of 500 ms to about 17,927 particles/μm^3 with a spot-to-plunge time of 100 ms (**Supplementary Figs. 4 & 5, Supplementary Videos 7 & 8**). Particle densities adsorbed to the air-water interfaces and the carbon substrate could not be interpreted in a straightforward way and understanding these behaviors requires further study.

These three example specimens show that deleterious effects of particle adsorption to air-water interfaces can be considerably reduced by decreasing the time between sample application and plunge-freezing, thus reducing the opportunities for particles to collide, adsorb, and equilibrate at air-water and substrate-water interfaces. In the case of increased non-adsorbed particles due to decreased spot-to-plunge time, recent software that is capable of accurately refining particle z-height locations within the ice[18–20] will provide the potential of separating non-adsorbed from adsorbed particles when calculating 3D maps. We anticipate that these interface effects can be further reduced by decreasing the spot-to-plunge time even further. The commercialized version of the Spotiton robot is expected to be capable of spot-to-plunge times as short as 20 ms.

METHODS

Methods are available in the Supplementary Methods section.

ACKNOWLEDGEMENTS
The authors wish to thank Prof. Robert Glaeser at Lawrence Berkeley National Laboratory for helpful discussions, Dr. Kotaro Kelley at the New York Structural Biology Center (NYSBC) for apoferritin purification, and the Electron Microscopy Group at NYSBC for microscope calibration and assistance.

This work was performed at the Simons Electron Microscopy Center and National Resource for Automated Molecular Microscopy located at the New York Structural Biology Center, supported by grants from the Simons Foundation (SF349247), NYSTAR, and the NIH National Institute of General Medical Sciences (GM103310) with additional support from the Agouron Institute (F00316) and NIH (OD019994).

AUTHOR CONTRIBUTIONS
A.J.N. collected and aligned tilt-series, and analyzed cryoET data. H.W. and V.P.D. performed the Spotiton experiments and the cryoEM experiments. H.W. made nanowire grids and collected tilt-series. H.W. and V.P.D. analyzed single particle cryoEM data. A.J.N., H.W., V.P.D., C.S.P., and B.C. conceived and designed the experiments. A.J.N. and B.C. wrote the manuscript.

COMPETING FINANCIAL INTERESTS
The authors declare no competing financial interests.

References

1. Nogales, E. The development of cryo-EM into a mainstream structural biology technique. *Nature Methods* (2015). doi:10.1038/nmeth.3694
2. Earl, L. A., Falconieri, V., Milne, J. L. & Subramaniam, S. Cryo-EM: beyond the microscope. *Curr. Opin. Struct. Biol.* **46,** 71–78 (2017).
3. Taylor, K. A. & Glaeser, R. M. Electron Diffraction of Frozen, Hydrated Protein Crystals. *Science* **186,** 1036–1037 (1974).
4. Adrian, M., Dubochet, J., Lepault, J. & McDowall, A. W. Cryo-electron microscopy of viruses. *Nature* **308,** 32–36 (1984).
5. Kühlbrandt, W. Biochemistry. The resolution revolution. *Science* **343,** 1443–1444 (2014).
6. Merk, A. *et al.* Breaking Cryo-EM Resolution Barriers to Facilitate Drug Discovery. *Cell* **165,** 1698–1707 (2016).
7. Noble, A. J. *et al.* Routine Single Particle CryoEM Sample and Grid Characterization by Tomography. (2017). doi:10.1101/230276
8. Glaeser, R. M. & Han, B.-G. Opinion: hazards faced by macromolecules when confined to thin aqueous films. *Biophys. Rep.* **3,** 1–7 (2017).
9. Naydenova, K. & Russo, C. J. Measuring the effects of particle orientation to improve the efficiency of electron cryomicroscopy. *Nat. Commun.* **8,** (2017).
10. Taylor, K. A. & Glaeser, R. M. Retrospective on the early development of cryoelectron microscopy of macromolecules and a prospective on opportunities for the future. *J. Struct. Biol.* **163,** 214–223 (2008).
11. Feng, X. *et al.* A Fast and Effective Microfluidic Spraying-Plunging Method for High-Resolution Single-Particle Cryo-EM. *Structure* **25,** 663-670.e3 (2017).
12. Jain, T., Sheehan, P., Crum, J., Carragher, B. & Potter, C. S. Spotiton: A prototype for an integrated inkjet dispense and vitrification system for cryo-TEM. *J. Struct. Biol.* **179,** 68–75 (2012).
13. Razinkov, I. *et al.* A new method for vitrifying samples for cryoEM. *J. Struct. Biol.* **195,** 190–198 (2016).
14. Dandey, V. P. *et al.* Spotiton: New Features and Applications. (2017). doi:10.1101/230151
15. Wei, H. *et al.* Optimizing “self-wicking” nanowire grids. *J. Struct. Biol.* (2018). doi:10.1016/j.jsb.2018.01.001
16. Scapin, G. *et al.* Structure of the Insulin Receptor–Insulin Complex by Single Particle CryoEM analysis. *Nature* (2018). doi:10.1038/nature26153
17. Tan, Y. Z. *et al.* Addressing preferred specimen orientation in single-particle cryo-EM through tilting. *Nat. Methods* **14,** 793–796 (2017).
18. Grigorieff, N., Grant, T. & Rohou, A. cisTEM: User-friendly software for single-particle image processing. *bioRxiv* 257618 (2018). doi:10.1101/257618
19. Zhang, K. Gctf: Real-time CTF determination and correction. *J. Struct. Biol.* **193,** 1–12 (2016).
20. Hu, M. *et al*. A Particle Filter Framework for Robust cryoEM 3D Reconstruction. Under review at Nature Methods (2018).

Figures

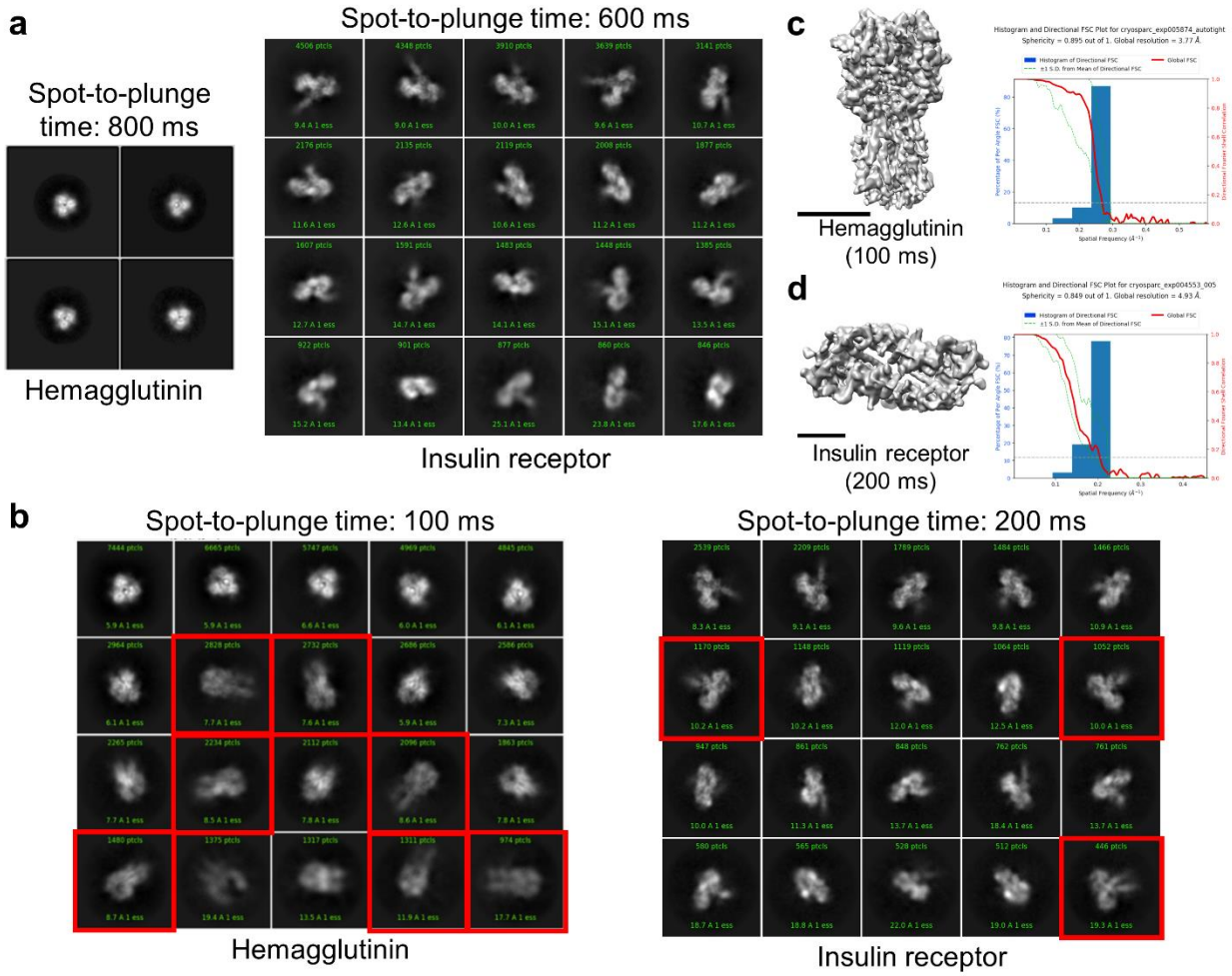

Figure 1 | Single particle cryoEM comparison between long and short spot-to-plunge times. (a) 2D classification of hemagglutinin with a spot-to-plunge time of 800 ms shows severe preferred orientation in the resulting 2D class averages, where only top-views of the elongated particle can be observed (left). 2D classification of insulin-bound insulin receptor with a spot-to-plunge time of 600 ms shows a more populated, yet incomplete, set of particle views in the class averages (right). (b) Spot-to-plunge times of 100 ms (left) for hemagglutinin and 200 ms (right) for insulin receptor recover the views of hemagglutinin and some additional side views of insulin receptor (red squares). (c) A 3.8 Å 3D reconstruction of hemagglutinin from the 100 ms spot-to-plunge dataset and its directional FSC plot confirm an acceptable isotropic distribution of particles orientations. (d) A 4.9 Å 3D reconstruction of insulin receptor from the 200 ms spot-to-plunge time dataset with its directional FSC plot. Scalebars are 5 nm.

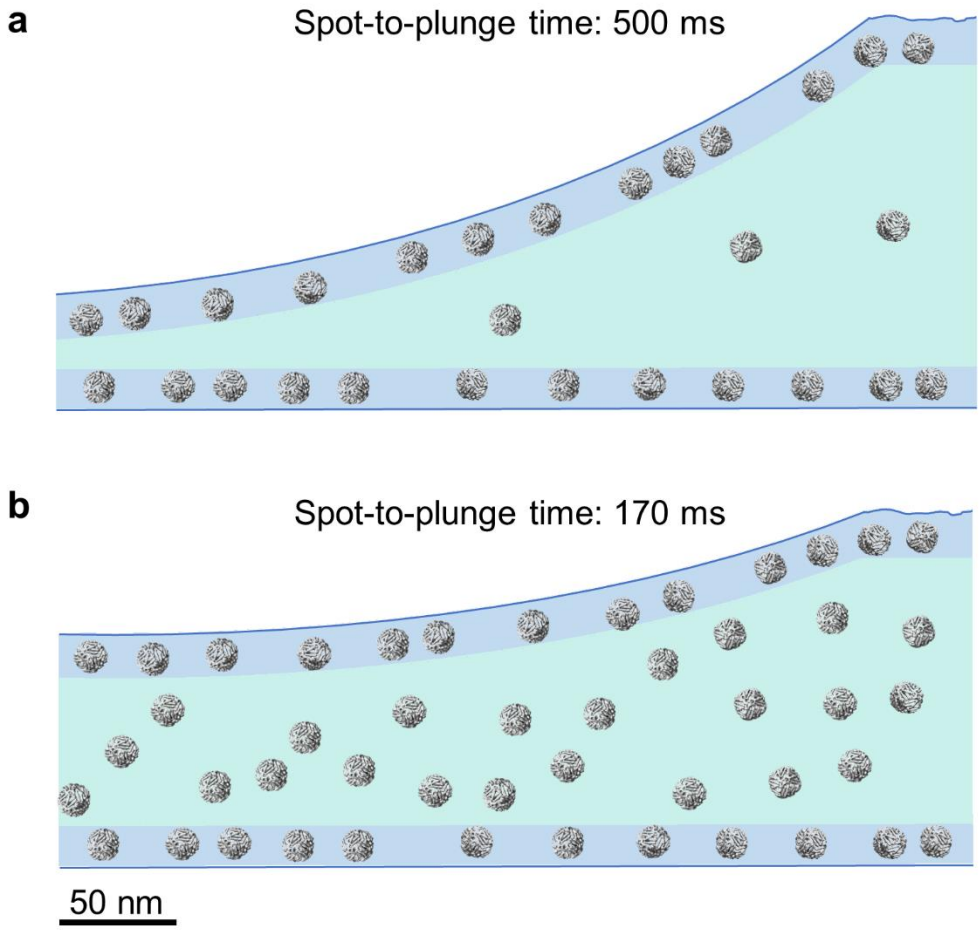

Figure 2 | CryoET cross-sectional depictions of apoferritin comparing long and short spot-to-plunge times. Areas colored in blue represent locations where particles are adsorbed to the air-water interface while areas in teal represent the volume in between. (a) Apoferritin with 0.5 mM TCEP (15 mg/mL = 20,530 particle/μm^3) plunged with a spot-to-plunge time of 500 ms shows that the vast majority of particles are adsorbed to air-water interfaces; the density of free-floating particles in the volume of ice is about 1,668 particles/μm^3. (b) Apoferritin plunged with a spot-to-plunge time of 170 ms shows that while many particles are still adsorbed to air-water interfaces, the density of free-floating particles in the volume of ice increased by about 20x to 31,725 particles/μm^3.

SUPPLEMENTARY METHODS

Sample preparation.

Hemagglutinin:
Hemagglutinin was prepared as described in Tan, Y. Z. et al., 2017[1].

Insulin-bound insulin receptor:
Insulin-bound insulin receptor was prepared as described in Scapin, G. et al., 2018[2].

Apoferritin:
Apoferritin from equine spleen (Sigma-Aldrich) as shown in **Figure 2, Supplementary Figures 1 & 3, and Supplementary Videos 3 & 6** was prepared by diluting the stock sample to 15 mg/mL with 0.5 mM TCEP.

Apoferritin from equine spleen (Sigma-Aldrich) as shown in **Supplementary Figures 4 & 5 and Supplementary Videos 7 & 8** was prepared as follows. 100 µL of sample at 25 mg/mL was diluted with 1 mL QA, 1 mL was loaded into a Q column, eluted with QB, and the main peak was pooled and concentrated to 0.5 mL. This 0.5 mL was then loaded onto a 10300 S200 column (GE) in QF, eluted at approximately 10.5 mL, and concentrated to working condition. [QA = 20 mM HEPES at pH 7.5, 0.1 mM EDTA at pH 8.0, 1 mM DTT; QB = QA + 1.5 M NaCl; QF = 150 mM NaCl, 20 mM HEPES at pH 7.5]

Grid preparation and vitrification:
Nanowire grids were prepared as described in Razinkov et al., 2016[3] and Wei et al., 2018[4].

The samples were vitrified using the semi-automated Spotiton V1.0 robot, a novel device for preparing cryoEM samples using piezo dispensing to apply small (50 pL) drops of sample across a “self-blotting” nanowire grid as it flies past *en route* to plunge into liquid ethane. Nanowire grids, manufactured in-house, backed by lacey carbon film supports were used for all experiments. Nanowire grids were plasma cleaned for 10 secs (O_2 + H_2) using a Solarus 950 (Gatan, Inc.). Sample was dispensed onto a grid dropping vertically past the dispense head in 50 pL drops for a total of ~5 nL of sample applied as a stripe across the grid which was then plunged into liquid ethane. The time between sample application to the grid and plunging into liquid ethane (spot-to-plunge time) ranged from 100 to 800 ms.

Single particle cryoEM data collection.

Hemagglutinin:
Single particle micrographs were collected on a Titan Krios (Thermo Fischer Scientific) equipped with an energy filter, Cs corrector, and a K2 counting camera (Gatan, Inc.); the microscope was operated at 300 kV at a nominal magnification of 130,000x, with a calibrated pixel size of 1.061 Å. Exposure was set to 10 secs (40 frames/image), for a total dose of 73.24

$e^-/Å^2$ with a defocus range of 1 to 2.1 µm. A total of 896 images were collected in three sessions using Leginon[5].

Insulin-bound insulin receptor:
Single particle micrographs were collected on a Titan Krios (Thermo Fischer Scientific) equipped with an energy filter and a K2 counting camera (Gatan, Inc.); the microscope was operated at 300 kV at a nominal magnification of 105,000x, with a calibrated pixel size of 1.096 Å. Exposure was set to 10 secs (40 frames/image), for a total dose of 66 $e^-/Å^2$ with a defocus range of 1 to 2.5 µm. Collection was performed over three sessions using Leginon. For the 200 ms spot-to-plunge experiment, a total of 1,526 micrographs were used for single particle processing while 1,866 micrographs were used for the 800 ms spot-to-plunge experiment.

Single particle cryoEM data processing.

Hemagglutinin:
Frames were aligned using MotionCor2[6]; global and per-particle CTF was estimated using gCTF[7]. Particle picking was performed using Gautomatch (http://www.mrc-lmb.cam.ac.uk/kzhang/) followed by one round of 2D refinement to remove false picks. A total of 104,365 particles were used for the final, symmetrized homogeneous 3D refinement in CryoSPARC[8], producing a 3.77 Å map as shown in **Figure 1c**.

Insulin-bound insulin receptor:
Micrograph frames were aligned using MotionCor2[6]; global and per-particle CTF was estimated using gCTF[7]. Particle picking was performed using Gautomatch (http://www.mrc-lmb.cam.ac.uk/kzhang/) followed by one round of 2D refinement to remove the false picks. Data processing from 2D classification through final reconstruction was performed using CryoSPARC as described in Scapin et al., 2018[2]. The completeness of the maps was assessed the Euler angle orientation distribution as calculated by CryoSPARC and by evaluating each map's 3D FSC.

For the 200 ms spot-to-plunge experiment, a total of 83,513 particles were selected for ab-initio 3D classification from which the best 40,390 particles were used for the final, symmetrized homogeneous 3D refinement, producing a 4.95 Å map.

For the 800 ms spot-to-plunge experiment, a total of 276,466 particles were selected for ab-initio 3D classification from which the best 70,276 particles were used for the final, symmetrized homogeneous 3D refinement, producing a 6.09 Å map.

Tilt-series data collection. Tilt-series were collected on a Titan Krios (Thermo Fischer Scientific) equipped with an energy filter and a K2 counting camera (Gatan, Inc.) and on a Tecnai F20 (Thermo Fischer Scientific) with a DE-20 camera (Direct Electron). Most tilt-series were collected nominally from -45° to 45° with 3° fixed or Saxton scheme[9] increments using either Leginon[5,10] or SerialEM[11] with a nominal defocus near 5 microns, per-tilt image doses

between 2 and 3 e-/Å^2, and a pixel size of 2.16 Å (K2) and 2.34 Å (DE-20). K2 tilt images were whole-frame aligned using MotionCor2.

Tilt-series data processing. Tilt-series were aligned with Appion-Protomo[12,13] by first dose compensating the images with respect to the total accumulated dose[14] of the tilt-series, coarse aligning tilt images, manually fixing coarse alignment if necessary, refining tilt-series alignment over several dozen iterations, and reconstructing with Tomo3D SIRT[15,16]. Tilt-series were not CTF corrected.

Tomogram particle picking. Particles in the apoferritin tomograms (**Supplementary Videos 3, 6, 7, & 8**) were picked manually using Dynamo[17]. Particle picks were separated by location: 1) Particles over the carbon in the zero-degree projection direction or adsorbed to the carbon, 2) Particles adsorbed to the air-water interfaces in the grid holes, and 3) Non-adsorbed particles in the grid holes. The particle picks and the resulting particle densities are shown in **Supplementary Figures 1, 3, 4, & 5**. Partial particles (where at least half of the particle is visible) were picked. We estimate that particle identification is accurate to within 1% and is complete to within 1% while volume measurements are estimated to be accurate to within 5% due to ice curvature and grid shape approximations, thus density calculations are likely accurate to within 5%.

References

1. Tan, Y. Z. *et al.* Addressing preferred specimen orientation in single-particle cryo-EM through tilting. *Nat. Methods* **14,** 793–796 (2017).
2. Scapin, G. *et al.* Structure of the Insulin Receptor–Insulin Complex by Single Particle CryoEM analysis. *Nature* (2018). doi:10.1038/nature26153
3. Razinkov, I. *et al.* A new method for vitrifying samples for cryoEM. *J. Struct. Biol.* **195,** 190–198 (2016).
4. Wei, H. *et al.* Optimizing “self-wicking” nanowire grids. *J. Struct. Biol.* (2018). doi:10.1016/j.jsb.2018.01.001
5. Stagg, S. *et al.* Applications of Automated Electron Microscopy: Using Leginon to Study the Structure of COPII Protein Complexes. *Microsc. Microanal.* **11,** 1072–1073 (2005).
6. Zheng, S. Q. *et al.* MotionCor2: anisotropic correction of beam-induced motion for improved cryo-electron microscopy. *Nat. Methods* **14,** 331–332 (2017).
7. Zhang, K. Gctf: Real-time CTF determination and correction. *J. Struct. Biol.* **193,** 1–12 (2016).
8. Punjani, A., Rubinstein, J. L., Fleet, D. J. & Brubaker, M. A. cryoSPARC: algorithms for rapid unsupervised cryo-EM structure determination. *Nat. Methods* **14,** 290–296 (2017).
9. Saxton, W. O., Baumeister, W. & Hahn, M. Three-dimensional reconstruction of imperfect two-dimensional crystals. *Ultramicroscopy* **13,** 57–70 (1984).
10. Suloway, C. *et al.* Fully automated, sequential tilt-series acquisition with Leginon. *J. Struct. Biol.* **167,** 11–18 (2009).
11. Mastronarde, D. N. SerialEM: A program for automated tilt series acquisition on Tecnai microscopes using prediction of specimen position. *Microsc. Microanal.* **9,** 1182CD (2003).
12. Noble, A. J. & Stagg, S. M. Automated batch fiducial-less tilt-series alignment in Appion using Protomo. *J. Struct. Biol.* **192,** 270–278 (2015).
13. Winkler, H. & Taylor, K. A. Accurate marker-free alignment with simultaneous geometry determination and reconstruction of tilt series in electron tomography. *Ultramicroscopy* **106,** 240–254 (2006).
14. Grant, T. & Grigorieff, N. Measuring the optimal exposure for single particle cryo-EM using a 2.6 Å reconstruction of rotavirus VP6. *eLife* **4,** e06980 (2015).
15. Agulleiro, J.-I. & Fernandez, J.-J. Tomo3D 2.0 – Exploitation of Advanced Vector eXtensions (AVX) for 3D reconstruction. *J. Struct. Biol.* **189,** 147–152 (2015).
16. Agulleiro, J. I. & Fernandez, J. J. Fast tomographic reconstruction on multicore computers. *Bioinforma. Oxf. Engl.* **27,** 582–583 (2011).
17. Castaño-Díez, D., Kudryashev, M., Arheit, M. & Stahlberg, H. Dynamo: A flexible, user-friendly development tool for subtomogram averaging of cryo-EM data in high-performance computing environments. *J. Struct. Biol.* **178,** 139–151 (2012).
18. Noble, A. J. *et al.* Routine Single Particle CryoEM Sample and Grid Characterization by Tomography. (2017). doi:10.1101/230276
19. Kremer, J. R., Mastronarde, D. N. & McIntosh, J. R. Computer Visualization of Three-Dimensional Image Data Using IMOD. *J. Struct. Biol.* **116,** 71–76 (1996).

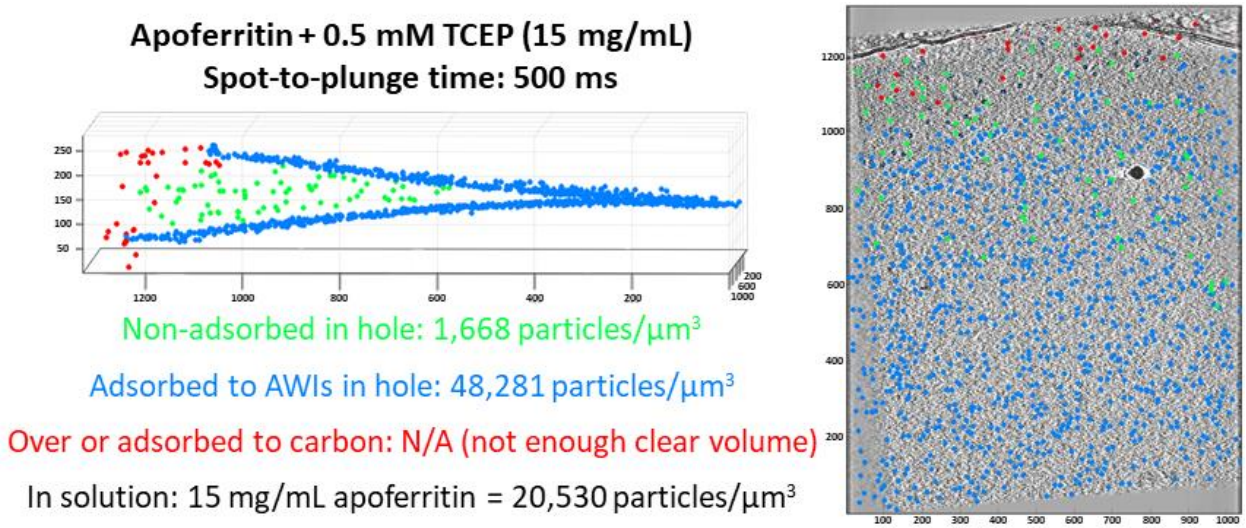

Supplementary Figure 1 | Particle distribution and concentrations of apoferritin (15 mg/mL = 20,530 particles/µm^3 in solution) with 0.5 mM TCEP prepared using Spotiton and nanowire grids with spot-to-plunge time of 500 ms. Particle picking and depictions were performed in Dynamo[17]. Left depiction is a side-view aligned roughly perpendicular to the air-water interfaces. Right depiction is a top-down view with a tomographic slice included. Particles were manually picked according to their estimated locations relative to the air-water interface and carbon. Calculated particle densities (particles/µm^3) are: 1,668 non-adsorbed in the hole and 48,281 adsorbed to the air-water interfaces. Particle concentration calculations are estimated to be accurate to within 5%. Scale: 100 pixels is ~86 nm.

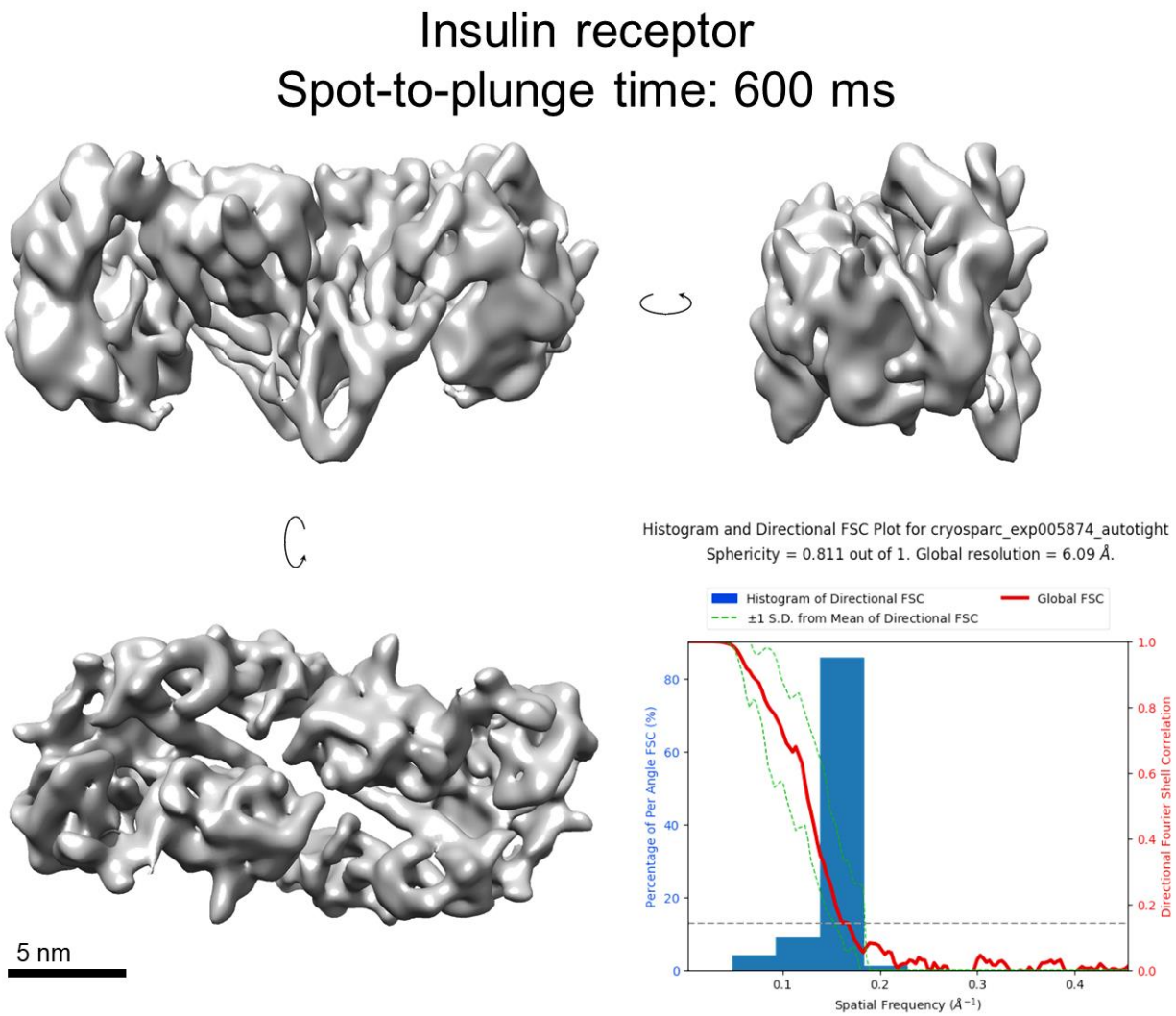

Supplementary Figure 2 | Single particle cryoEM of insulin-bound insulin receptor with a longer spot-to-plunge time of 600 ms. As shown in **Figure 1**, some side views of insulin receptor are missing in the class averages of the 600 ms spot-to-plunge preparation. This resulted in a reduced sphericity of the 3D FSC (0.811 vs. 0.849 for the 200 ms spot-to-plunge time) and worse resolution in the calculated map (6.09 Å vs. 4.93 Å for 200 ms). The anisotropy associated with for the longer spot-to-plunge time is reflected in the stretching artifacts in the 3D reconstruction.

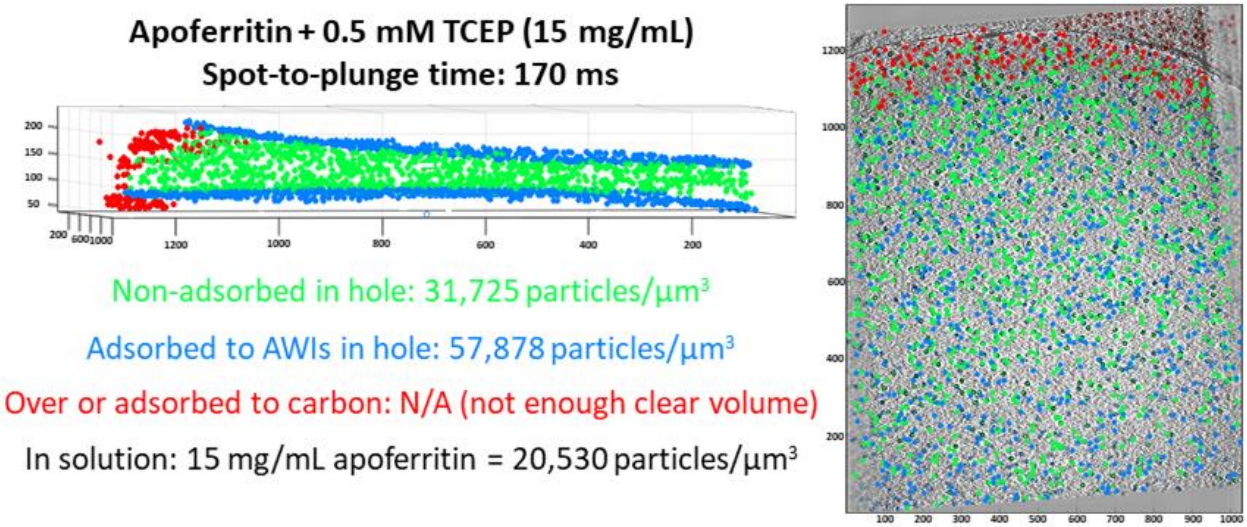

Supplementary Figure 3 | Particle distribution and concentrations of apoferritin (15 mg/mL = 20,530 particles/µm^3 in solution) with 0.5 mM TCEP prepared using Spotiton and nanowire grids with spot-to-plunge time of 170 ms. Left depiction is a side-view aligned roughly perpendicular to the air-water interfaces. Right depiction is a top-down view with a tomographic slice included. Particles were manually picked according to their estimated locations relative to the air-water interface and carbon. Calculated particle densities (particles/µm^3) are: 31,725 in the hole and 57,878 adsorbed to the air-water interfaces. Particle concentration calculations are estimated to be accurate to within 5%. Scale: 100 pixels is ~86 nm.

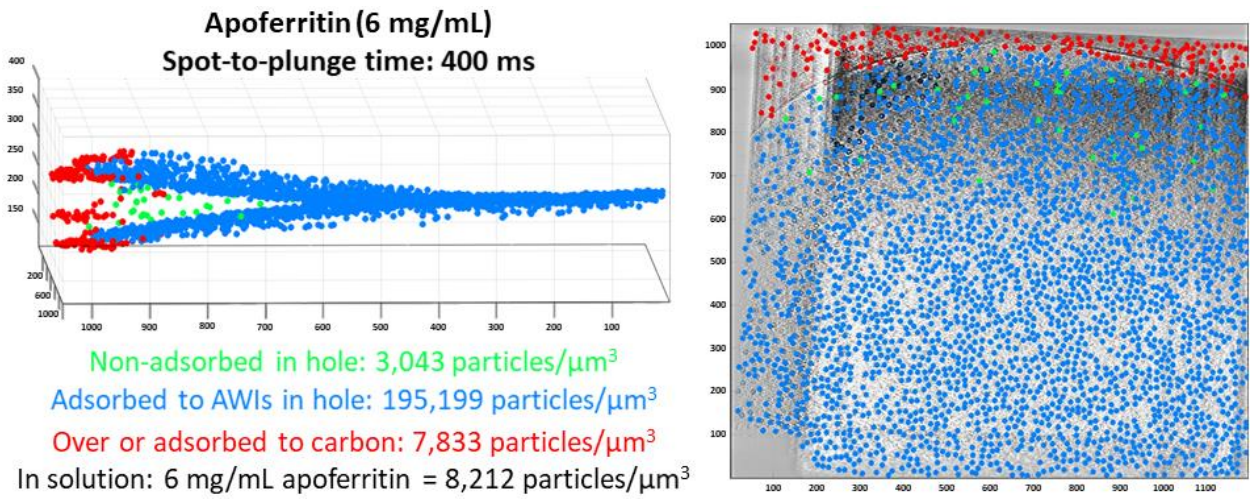

Supplementary Figure 4 | Particle distribution and concentrations of apoferritin (6 mg/mL = 8,212 particles/µm^3 in solution) prepared using Spotiton and nanowire grids with spot-to-plunge time of 400 ms. Left depiction is a side-view aligned roughly perpendicular to the air-water interfaces. Right depiction is a top-down view with a tomographic slice included. Particles were manually picked according to their estimated locations relative to the air-water interface and carbon. Calculated particle densities (particles/µm^3) are: 3,043 in the hole, 195,199 adsorbed to the air-water interfaces, and 7,833 over or adsorbed to carbon. Particle concentration calculations are estimated to be accurate to within 5%. Scale: 100 pixels is ~86 nm.

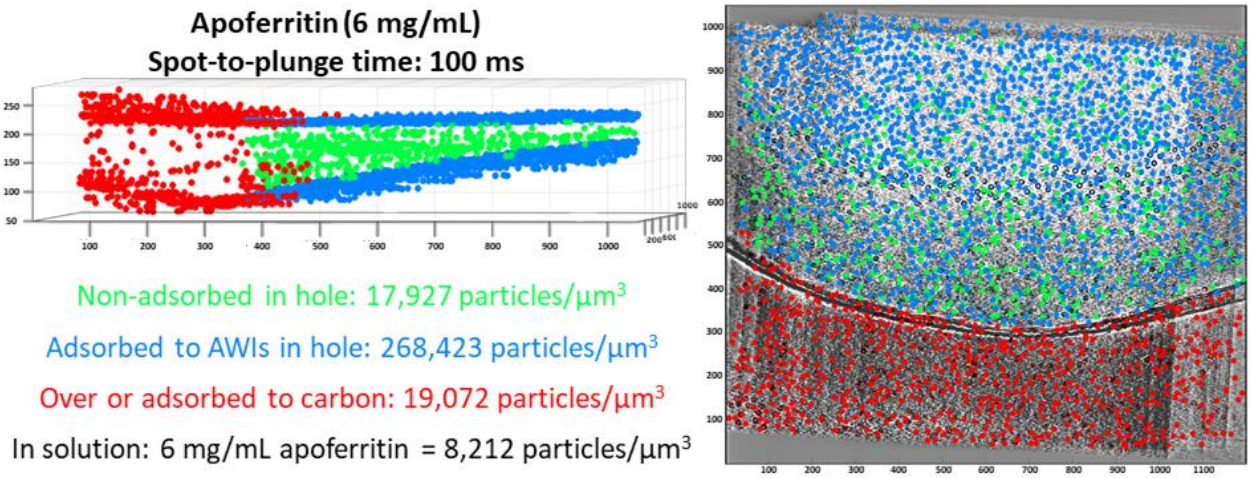

Supplementary Figure 5 | Particle distribution and concentrations of apoferritin (6 mg/mL = 8,212 particles/µm^3 in solution) prepared using Spotiton and nanowire grids with spot-to-plunge time of 100 ms. Left depiction is a side-view aligned roughly perpendicular to the air-water interfaces. Right depiction is a top-down view with a tomographic slice included. Particles were manually picked according to their estimated locations relative to the air-water interface and carbon. Calculated particle densities (particles/µm^3) are: 17,927 in the hole, 268,423 adsorbed to the air-water interfaces, and 19,072 over or adsorbed to carbon. Particle concentration calculations are estimated to be accurate to within 5%. Scale: 100 pixels is ~86 nm.

Supplementary Videos

Supplementary Video 1 | Tomogram slice-through of hemagglutinin prepared using Spotiton and nanowire grids with spot-to-plunge time of 800 ms, alongside a cross-sectional depiction. The vast majority of particles are observed to be adsorbed to the air-water interfaces with severe preferred orientation. Slice-through videos were rendered using 'Slicer' 3dmod from the IMOD package[19] by orienting one plane of particles at the air-water interface to be roughly parallel to the field of view.

Supplementary Video 2 | Tomogram slice-through of insulin-bound insulin receptor prepared using Spotiton and nanowire grids with spot-to-plunge time of 600 ms, alongside a cross-sectional depiction. The vast majority of particles are observed to be adsorbed to the air-water interfaces.

Supplementary Video 3 | Tomogram slice-through of apoferritin with 0.5 mM TCEP (15 mg/mL) prepared using Spotiton and nanowire grids with spot-to-plunge time of 500 ms, alongside a cross-sectional depiction. Most of particles are observed to be adsorbed to the air-water interfaces, with a few non-adsorbed particles.

Supplementary Video 4 | Tomogram slice-through of hemagglutinin prepared using Spotiton and nanowire grids with spot-to-plunge time of 100 ms, alongside a cross-sectional depiction. A majority of the particles are observed to be adsorbed to the air-water interfaces.

Supplementary Video 5 | Tomogram slice-through of insulin-bound insulin receptor prepared using Spotiton and nanowire grids with spot-to-plunge time of 200 ms, alongside a cross-sectional depiction.

Supplementary Video 6 | Tomogram slice-through of apoferritin with 0.5 mM TCEP (15 mg/mL) prepared using Spotiton and nanowire grids with spot-to-plunge time of 170 ms, alongside a cross-sectional depiction. Approximately nineteen times as many non-adsorbed particles are in the field of view as compared to the spot-to-plunge time of 500 ms (**Supplementary Video 3**).

Supplementary Video 7 | Tomogram slice-through of apoferritin (6 mg/mL) prepared using Spotiton and nanowire grids with spot-to-plunge time of 400 ms, alongside a cross-sectional depiction. Most of the particles are observed to be adsorbed to the air-water interfaces, with a few non-adsorbed particles.

Supplementary Video 8 | Tomogram slice-through of apoferritin (6 mg/mL) prepared using Spotiton and nanowire grids with spot-to-plunge time of 100 ms, alongside a cross-sectional depiction. Approximately six times as many non-adsorbed particles are in the field of view as compared to the spot-to-plunge time of 400 ms (**Supplementary Video 7**).